Measurements of molecular-frame Auger electron angular distributions at the CO C $1s^{-1}$ $2\pi^*$ resonance with high energy resolution

2008 J. Phys. B: At. Mol. Opt. Phys. 41 215101

(http://iopscience.iop.org/0953-4075/41/21/215101)

J. Phys. B: At. Mol. Opt. Phys. **41** (2008) 215101 (11pp) doi:10.1088/0953-4075/41/21/215101

Measurements of molecular-frame Auger electron angular distributions at the CO C $1s^{-1}$ $2\pi^*$ resonance with high energy resolution

G Prümper[1], D Rolles[2,3], H Fukuzawa[1], X J Liu[1], Z Pešić[2,3], I Dumitriu[2,3], R R Lucchese[4], K Ueda[1] and N Berrah[2]

[1] Institute of Multidisciplinary Research for Advanced Materials, Tohoku University, Sendai 980–8577, Japan
[2] Physics Deptartment, Western Michigan University, Kalamazoo, MI 49008, USA
[3] Advanced Light Source, Lawrence Berkeley National Laboratory, Berkeley, CA 94720, USA
[4] Department of Chemistry, Texas A&M University, College Station, TX 77843-3255, USA

Received 11 July 2008, in final form 3 September 2008
Published 13 October 2008
Online at stacks.iop.org/JPhysB/41/215101

Abstract
The molecular-frame Auger electron angular distributions (MFAEADs) of resonantly excited CO 1s $\rightarrow \pi$ molecules in the gas phase were determined with high energy resolution using a novel experimental approach. We investigated the process of excitation, Auger decay and fragmentation in unprecedented detail. We confirmed theoretical predictions for the different MFAEADs of close lying Auger final states. By examining the dependence of the MFAEADs on the vibrational state of the excitation and on the fragmentation energy we found that the measured MFAEADs can be considered independent of the vibrational excitation and the fragmentation process. The method used to obtain molecular-frame angular distributions of Auger electrons is based on electron–ion coincidence measurements using two high-resolution electron spectrometers with limited acceptance angles mounted at fixed positions.

1. Introduction

Resonant Auger decay in molecules is a fascinating process, even in the simplest case of a diatomic molecule such as CO exposed to low-intensity linearly polarized radiation. Single photon absorption leading to a 1s core hole and Auger decay involves many aspects of electronic and nuclear dynamics. Let us start with the electronic dynamics: unlike in the normal Auger decay resonant photoabsorption populates a valence level which stays occupied until the Auger decay occurs—or in the case of spectator Auger decay, even until after the first Auger decay. Therefore the information about the polarization direction of the ionizing radiation is not carried away by a photoelectron but is stored inside the excited molecule in the form of the alignment of the excited orbital. Therefore in contrast to the normal Auger decay, for resonant Auger electron emission the angular distribution typically shows a strong dependence on the polarization direction of the radiation. In many ways resonant Auger decay is more closely related to direct photoionization than to the normal Auger decay and the distinction between resonant Auger electrons and photoelectrons is somewhat artificial and reflects merely our way of thinking about the process and not the outcome of the process itself. In both cases one photon is absorbed, one electron is emitted and a singly charged molecular ion is left behind, either in its ground state or an excited state. The resonant Auger decay may lead to many different final electronic states depending which orbitals are depleted when the core hole is filled and an Auger electron is emitted. The molecular frame is the natural coordinate system to discuss the emission electrons as the molecular potential influences the angular distributions (ADs) very strongly as demonstrated in recent showcase experiments (Weber *et al* 2004, Rolles *et al* 2005) on doubly charged final states. Some of the potential's effects can be thought of as intramolecular scattering, reflections or lens effects on the outgoing electrons. As the different possible paths of the electron through the molecule are generally indistinguishable, the ADs contain

strong interference patterns. The AD for each normal or resonant Auger final state is therefore a complicated function of the emission angles. There has been a steady progress in the theoretical description of MFAEADs of normal Auger electrons (Zähringer *et al* 1992b, Kuznetsov and Cherepkov 1996, Bonhoff *et al* 1997, Semenov *et al* 2007, Zähringer *et al* 1992a, Edwards *et al* 1997) but only few experimental studies of MFAEADs are available (Guillemin *et al* 2001, Weber *et al* 2003). Both of them deal with the CO normal Auger decay but the results are highly contradictory.

Recent progress in the theoretical description (Bonhoff *et al* 1999) has made it possible to calculate also the ADs of resonant Auger electrons for simple molecules such as CO. The theoretical model contains several simplifying assumptions, such as the one-centre approach and a simplified treatment of the effects of the molecular potential. Our experiment serves as a benchmark test for these predictions. The first question is therefore, how good is the agreement between the theoretical prediction and the experiment?

Taking the nuclear dynamics into account, further questions arise. With current synchrotron light sources it is easily possible to tune the wavelength of the ionizing radiation to resonances that lead to the vibrational ground state ($\nu = 0$) at a photon energy of $h\nu = 287.40$ eV of the excited CO molecule or to its first excited state ($\nu = 1$) at $h\nu = 287.66$ eV. As the vibrational structure in the resonance profile of the total ion yield indicates, the core excited state of the molecule lives long enough to undergo several vibrations before the resonant Auger decay happens. Therefore the nuclear dynamics might also have some influence on the resonant Auger decay. It is well known that the resonant Auger spectrum changes shape with the vibrational excitation level, as the individual transition rates to the different final electronic states depend critically on the internuclear distance, whose average value changes with the vibrational level. This leads to our second question: do the MFAEADs depend on the vibrational level of the excited state?

Resonant Auger decay can lead to dissociative electronic states of the molecular ion. Each of the many possible electronic states has its own potential curve and the dissociation can, for example, lead to C^+–O pairs, with different asymptotic velocities and internal excitations of the fragments. The dissociation pathway certainly depends on the initial vibrational state of the molecule. In classical terms this corresponds to different starting points and velocities on the potential surfaces, while in a quantum-mechanical description the initial state of the nuclear wavefunctions is different. Certainly the outcome of the dissociation depends on the final state of the resonant Auger decay as it determines the initial potential curve of the dissociation. Nevertheless one expects that the dynamics during the dissociation, for example diabatic crossing to another potential curve leading to C^+ and O with different kinetic energies, can no longer influence the Auger electron. On the other hand, the resonantly emitted Auger electron leaves behind valence holes in the singly charged molecular ion. In general, a correlation of the electron emission direction and an alignment of the valence hole states must be expected. These valence holes can affect the dissociation process. Translated into measurable quantities this leads to the third question: for a fixed resonant Auger final state, is the kinetic energy release of the fragments correlated to the MFAEADs?

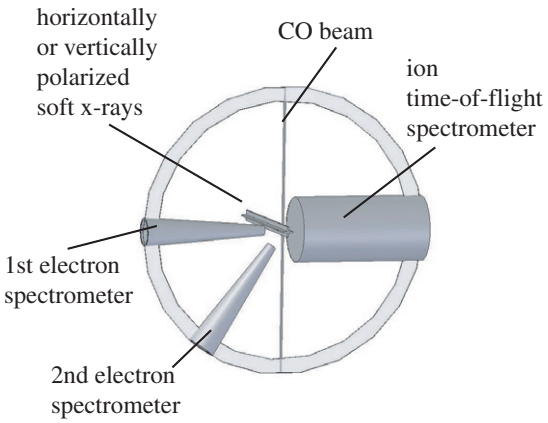

Figure 1. Schematic of the experimental apparatus. Looking towards the synchrotron radiation source. The vacuum chamber contains a source for a supersonic CO jet, two electron TOF spectrometers and a pulsed-field ion spectrometer for the momentum determination of the C^+ ions. The jet and the spectrometer axes are all in one plane perpendicular to the light propagation direction, symbolized by the ring. The first electron spectrometer is mounted horizontally, the second one at 54.7° with respect to the horizontal. The light polarization can be switched between horizontal and vertical.

2. Experiment

A supersonic beam source for CO molecules was mounted inside a vacuum chamber and installed at beamline 4.0.1 of the advanced light source (ALS) at Lawrence Berkeley National Laboratory. The molecular beam was produced by an expansion of room temperature CO gas with a stagnation pressure of 1 atm through a 70 μm orifice.

For each photon energy we made two measurements using linearly polarized radiation, with the electric vector oscillating in the horizontal and the vertical directions, respectively. Two angle and kinetic energy resolving electron time-of-flight (TOF) spectrometers were mounted in the plane perpendicular to the propagation direction of the light. This is illustrated in figure 1. This plane also contains the source of the CO beam and an ion TOF spectrometer that will be described below. One electron TOF spectrometer is mounted in the horizontal direction. The second spectrometer detects electrons emitted at 54.7° with respect to the horizontal. Technical details about the electron spectrometers can be found in Berrah *et al* (1999). The TOF spectrometers have a length of 689 mm from the source volume to the electron detector. We applied a retarding voltage of 244.4V to obtain an instrumental energy resolution of about 300 meV. The filling mode of the storage ring of the ALS was the two-bunch operation leaving a sufficient time gap between the light pulses, so slow electrons originating from one light pulse reach the detector before fast electrons from the next pulse. Under typical experimental conditions the electron count rate in the relevant kinetic energy interval (259–261 eV)

of the Auger electrons was about 0.4 Hz. The data acquisition was performed as described in the following paragraph.

Whenever one of the two electron spectrometers detects an electron, an 8 channel time-to-digital converter (TDC) module is started. The TDC module has a time resolution of 500 ps. This module records the information, about which electron spectrometer provided the start pulse and the time of the following bunch marker signal (BMS), an electronic signal that resembles the timing of the light pulses with a fixed delay. For a known delay, the time of flight of the electron and its kinetic energy can be deduced from the recorded information. Electron TOF and energy spectra can be generated in an off-line analysis. After the detection of each electron a pulsed electric field is applied to the electrodes of the ion spectrometer with a fixed delay of 540 ns with respect to the light pulse. The CO^+ or the C^+ ion which has travelled only a few mm during the 540 ns is extracted towards the position resolving ion detector. The ion TOF and the ion detector hit position are recorded together with the electron data. Our experimental setup is essentially a technically improved version of the experimental setup described in Golovin *et al* (1997), Heiser *et al* (1997) that is based on the pioneering works of Golovin and coworkers (Golovin *et al* 1992). The electron and the ion do not necessarily come from the same molecule. We gathered reference data for the subtraction of the contributions from such random coincidences, by using a 100 Hz pulse generator that triggered the TDC module and the high voltage (HV) pulse generator. A detailed description of the method can be found in Prümper and Ueda (2007). In the present work all figures show the data after subtraction of the random coincidence contribution.

The ion spectrometer is a modified version of the spectrometer described in Rolles *et al* (2007). It consists of four electrodes named pusher, extractor, lens and drift tube. The pusher, extractor and lens electrodes are flat ring-shaped electrodes with outer diameters of 40 mm and inner diameters of 30 mm. The distance between the pusher electrode to the extractor electrode is 18 mm. The pusher and extractor electrodes are covered with flat stainless steel meshes in order to obtain a homogeneous electric field between them, when the HV pulse of +270 V is applied to the pusher while the extractor stays grounded for simplicity. A 340 mm long aluminium drift tube is mounted 42 mm behind the extractor electrode. It has flat grids of the same type like the pusher and extractor electrodes on both ends to guarantee a field free drift region inside the drift tube. A pulsed voltage of −950 V is applied to it. Between extractor and drift tube (19 mm away from the extractor) a ring-shaped lens electrode is mounted. It also has an outer diameter of 40 mm and an inner diameter of 30 mm. A pulsed voltage of −370 V is applied to achieve the velocity focusing condition, i.e. for a given mass and charge state the hit position on the detector depends only on the momentum of the ion but not on its starting position. A very similar instrument, based on a design of Lebech and coworkers (Lebech *et al* 2002), is described in detail in Prümper *et al* (2007). There the method for calculating the initial ion momentum from the TOF and the hit position is described for the case of the inhomogeneous field in the lens region. In this experiment, velocity focusing is not a critical condition because the intersection of the light beam with the gas jet defines a fairly small source volume. The main advantage of using the lens element is an extended kinetic energy range for which the spectrometer has a 4π sr collection efficiency for the given ion detector area of 75 mm diameter. The whole ion spectrometer is contained in a grounded tube to have well-defined boundary conditions for the electric field and to shield the electron detectors against the noise from the switching of the HV extraction fields.

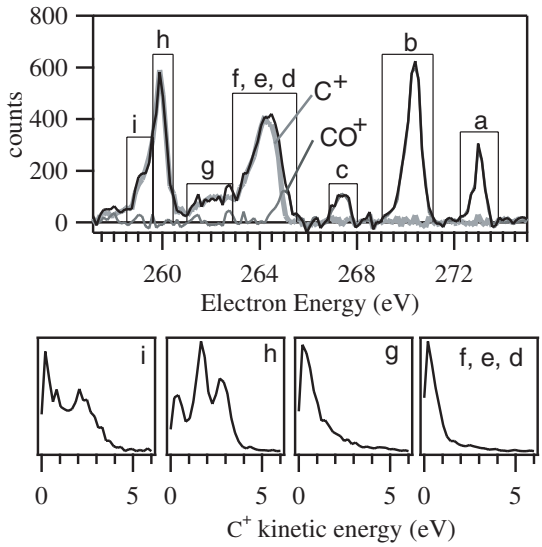

Figure 2. Auger electron energy spectrum for the C(1s) → π excitation to the first excited vibrational state. $\nu = 0$ at $h\nu =$ 287.40 eV. Upper panel: electron spectra recorded in detector 2 at 54.7° for horizontally polarized light, in coincidence with C^+ ions (thick grey line) or CO^+ ions (thin grey line). The sum of both (black line) resembles the non-coincident electron spectrum. The energy axis of the spectrum contains intervals a–i, corresponding to the main features. The lower panels show the kinetic energy distribution of the C^+ ions for the corresponding intervals. The total kinetic energy release is 1.75 times the kinetic energy of the C^+ ions.

3. Results

3.1. Electron spectrum

From the data recorded with light polarized in the horizontal direction, we created an electron energy spectrum for the electron spectrometer 2 that is mounted at 54.7° with respect to the electric vector of the light. This spectrum is shown in figure 2. The nonlinear function to translate the TOF into kinetic energy was chosen in a way to get the best overall agreement with the high-resolution spectra in Piancastelli *et al* (1997). Using the coincidence information, the electron spectrum can be disentangled with respect to the ions produced. In this case only two types of ions are found in coincidence with the Auger electrons: C^+ and CO^+. The small diagrams in figure 2 show the corresponding distributions of the kinetic energies of the C^+ ions for each Auger band. The bands are labelled a–i according to Bonhoff *et al* (1999).

The resonant Auger electron spectrum has been studied extensively before (Piancastelli *et al* 1997, Kukk *et al* 1999).

We will only give a brief summary of the main features. At a photon energy of 287.40 eV the C 1s core electron is promoted to the lowest unoccupied molecular orbital LUMO. The LUMO has π-symmetry, so in the excitation process molecules with their axes oriented parallel to the light polarization will not be excited. For the Auger decay many different electronic final states are possible. The electrons with the highest kinetic energy, here labelled as a, b and c, belong to the participator decays (Svensson *et al* 1991, Hemmers *et al* 1993) where the π electron from the LUMO is emitted and an electron from the valence states fills the core hole (or vice versa). All these electronic states belong to CO^+ molecules that do not fragment (Westerveld *et al* 1996), also seen in our coincidence data. The slightly less energetic Auger electrons belong to spectator Auger decays where the excited electron stays in the π-orbital and the decay leads to a double vacancy in the valence orbitals. These states lead to fragmentation into C^+ and O. The corresponding C^+ energy spectra are shown in the lower row of figure 2. The d–g states lead to C^+ ions with less than 1 eV of kinetic energy, while the h and i states lead to energetic fragmentation where the C^+ ion gains up to 5 eV of kinetic energy. Previous studies (Botting and Lucchese 1997, Piancastelli *et al* 1997, Feyer *et al* 2007) assigned the h-band to the $4\sigma^{-1}5\sigma^{-1}2\pi^2\Pi$-state, while the assignment for the i-band is not unique (Osborne *et al* 1998, Feifel *et al* 2002). The total kinetic energy release (TKER) is 1.75 times the kinetic energy of the C^+ ion so, for example, the peak at 3 eV for the h-band belongs to a TKER of 5.25 eV. This value is larger than the value of 4 eV derived from the potential curves shown in Piancastelli *et al* (1997) figure 1, assuming that the crossing between the potential curves are forbidden.

3.2. Theoretical predictions and assignments

The aim of this work is to determine the molecular-frame Auger electron angular distributions (MFAEADs). Let us start by defining the molecular frame more precisely: in case of diatomic molecules such as CO only one molecular axis $\vec{n}$ pointing from O to C is important. Imagine a sample of molecules that has a well-defined direction of the molecular axis, all pointing with the carbon atom in the positive z-direction. Even through the polarization direction of the light does not give us a preferential orientation, we arbitrarily choose an oriented vector $\vec{E}$ as a reference direction. The coordinate frame x, y, z is chosen in a way that $\vec{E}$ is in the x–z-plane, with a positive x-component. We define the angle θ_n^E between the molecular axis $\vec{n}$ and $\vec{E}$,

$$\theta_n^E = \arccos(\vec{E}, \vec{n}). \tag{1}$$

So the values of θ_n^E are not restricted to the interval from 0° to 90° but can take values from 0° to 180°.

The ionization cross section may strongly depend on θ_n^E for resonant processes. Electrons can be emitted in all directions. Their directions $\vec{e}$ are described by two spherical angles θ and ϕ_n. θ is the angle between $\vec{e}$ and $\vec{n}$. ϕ_n is the angle in the x, y-plane. θ can take values from 0° to 180°, ϕ_n can take values from 0° to 360°.

Table 1. Angular distribution parameters predicted by theory (Fink *et al* submitted)

	$3^2\Pi$	$4^2\Pi$	$5^2\Pi$	$1^2\Phi$
$A_0(1,1)$	4.995 279	5.035 757	0.635 149	0.456 637
$A_1(1,1)$	−6.655 709	−6.006 927	0.760 373	0.000 050
$A_2(1,1)$	2.216 655	1.591 107	0.778 837	−0.651 948
$A_3(1,1)$	−0.900 415	−0.225 360	−0.187 053	0.000 021
$A_4(1,1)$	0.415 597	0.296 497	0.056 594	0.195 825
$A_2(-1,1)$	−0.347 476	0.764 852	0.007 624	0
$A_3(-1,1)$	−0.315 657	1.419 963	0.031 787	0
$A_4(-1,1)$	0.243 367	−0.250 590	−0.016 515	0

Therefore the intensity distribution of electrons in the molecular frame can be expressed as a function of three variables: $I^m(\theta_n^E, \theta, \phi_n)$.

Table 1 summarizes parameters to describe the MFAEADs prediction by Fink and coworkers (Fink *et al* 2008) for the four relevant final ionic states. For each state the AD is given by equation (2)

$$I(\theta_n^E, \theta, \phi_m) = \sin^2(\theta_n^E) \cdot \left(\sum_k A_k(1,1) \cdot P_k^0(\cos(\theta)) - \sum_k f_k \cdot A_k(1,-1) \cdot P_k^2(\cos(\theta)) \cdot \cos(2\phi_m) \right)$$
$$\text{with} \quad f_2 = \frac{1}{\sqrt{24}}, \quad f_3 = \frac{1}{\sqrt{120}}, \quad f_4 = \frac{1}{\sqrt{360}}. \tag{2}$$

The total transition intensity for each line is proportional to $A_0(1,1)$. The h-band has contributions from the $3^2\Pi$ and $4^2\Pi$ states, the i-band has contributions form the $4^2\Pi$ and $5^2\Pi$ and $1^2\Phi$ states (Fink *et al* 2008). The variable x describes the branching ratio of the $4^2\Pi$ state contributes into the h-band and the i-band

$$I_h = I_{3^2\Pi} + x \cdot I_{4^2\Pi} \tag{3}$$
$$I_i = (1-x) \cdot I_{4^2\Pi} + I_{5^2\Pi} + I_{1^2\Phi}. \tag{4}$$

We estimated the value of x from the measured intensity ratio of the h-band and the i-band. Because of the better resolution and statistics, conventional spectra (Piancastelli *et al* 1996) were used for this purpose. The high-resolution spectrum recorded at the magic angle is in good agreement with our data, when it is convoluted by a Gaussian peak of 300 meV FWHM to model the lower resolution in our experiment. Based on a simple fitting of the data by two Gaussian peaks with different widths we estimate the h/i intensity ratio as 2.37:1. From this result and the values of $A_0(1,1)$ in table 1 we calculate $x = 0.561$. The ADs of the states $3^2\Pi$ and $4^2\Pi$ are very similar. The ADs of the $4^2\Pi$ and $5^2\Pi$ and $1^2\Phi$ states are very different. Therefore the AD of the h-band does not depend on the value of x very much, while the AD of the i-band does. The theoretical prediction of the AD for the h-band is more reliable than that for the i-band. The $4^2\Pi$ state has a much larger value for $A_0(1,1)$ compared to $5^2\Pi$ and $1^2\Phi$ states. Therefore the AD of the i-band has a strong contribution that looks like the AD of the h-band plus two very different additional contributions. In the experiment one may consider additional mixing of the h-band and i-band

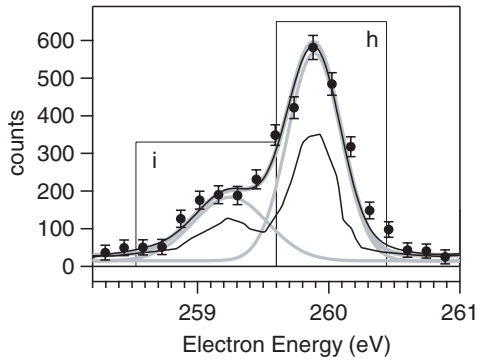

Figure 3. Analysis of the overlapping h- and i-bands. The black data points are from our coincidence measurement. The black boxes show the intervals used for the data analysis. The lower black line shows the high-resolution data of Piancastelli and coworkers (Piancastelli *et al* 1997), scaled arbitrarily. To mimic the effect of our lower instrumental resolution we convoluted the data with a 300 meV FWHM Gaussian profile (upper black line). This value gives the best overall agreement with our measured electron spectrum. This convoluted spectrum can easily be fitted by a double-peak structure (grey lines) + a constant background.

contributions due to limited experimental resolution. For the sake of simplicity this minor effect is not considered here.

3.3. Experimental angular distributions

Our method to determine the orientation of the free CO molecules at the instant of photo-excitation is the so-called fixed-in-space method (Golovin *et al* 1992, 1997, Shigemasa *et al* 1995, Heiser *et al* 1997, Dörner *et al* 1998, Downie and Powis 1999). It relies on the axial recoil approximation. We determine the momentum of one ionic fragment, e.g. C^+, and assume that it coincides with the molecular axis in the time interval from the excitation to the Auger decay.

In order to determine the direction of this molecular axis, we need to determine the momenta of the ions. Therefore we need to choose experimental conditions where the detector is almost fully illuminated by energetic ions. Otherwise the position information is not precise enough. The experimental condition were set in a way, that we can determine the momentum direction of C^+ ions in the kinetic energy interval from 1 eV to 6 eV with sufficiently high precision. Therefore we chose to consider the ADs of Auger electrons for the i-state and the h-state only. This choice is purely technical in nature. We do not want to imply that the axial recoil approximation breaks down for the d–g band shown in figure 2. Unless stated otherwise, the angular distributions shown in this work refer to the kinetic energy interval of C^+ ions form 1.0 eV to 6.0 eV.

Note that having a small source region or a velocity focusing condition, it is sufficient to detect one ionic fragment to determine the molecular axis. This is essential as the resonant Auger decay does not produce ion pairs.

We will use a somewhat indirect method to determine the MFAEADs experimentally. For this we need to take a closer look at the general form of the MFAEADs. As a consequence of the dipole approximation this three-dimensional function $I^m\left(\theta_n^E, \theta, \phi_n\right)$ can be written in terms of four one-dimensional functions: $F_{00}^{(m)}(\theta)$, $F_{20}^{(m)}(\theta)$, $F_{21}^{(m)}(\theta)$ and $F_{22}^{(m)}(\theta)$ which is a tremendous simplification of the problem (Lucchese *et al* 2002):

$$I^m\left(\theta_n^E, \theta, \phi_n\right) = F_{00}^{(m)}(\theta) + \tfrac{1}{2}\left(3\cos^2\left(\theta_n^E\right) - 1\right) \cdot F_{20}^{(m)}(\theta) + 3\sin\left(\theta_n^E\right)\cos\left(\theta_n^E\right) \cdot F_{21}^{(m)}(\theta) \cdot \cos\left(\phi_n\right) + 3\sin^2\left(\theta_n^E\right) \cdot F_{22}^{(m)}(\theta) \cdot \cos\left(2\phi_n\right). \quad (5)$$

This formula applies for the direct photoionization process and resonant Auger decay. In theory there is no distinction between the two processes. Coulomb interaction between all electrons in the molecule is included at every photon energy. Therefore equation (5) is consistent with the Kramers–Heisenberg formula for singly charged final states. In general the ADs can depend explicitly on the angle θ_n^E. Equation (2) is a special case of equation (5) just as the two-step model is a special case of the Kramers–Heisenberg formula. Equation (2) is based on the two-step model, therefore the dependance on θ_n^E appears just as a scaling factor. In this paper we test if the experimentally measured MFAEAD need to be described by the general equation (5) or if they can be reduced to the simple form given by equation (2). By comparing the measured MFEAD with the theoretical predictions we will show, that not only the description by equation (2) is a good approximation, but that the theoretical calculation also yields correct values for the parameters $A_k(1, 1)$ and $A_k(1, -1)$.

The general equation (5) does not only describe the angular distributions for fixed values of θ_n^E but also the variation of the total ionization cross section as a function of θ_n^E, i.e. the selectively of the molecular axis in the absorption process. Once $F_{00}^{(m)}$, $F_{20}^{(m)}$, $F_{21}^{(m)}$, $F_{22}^{(m)}$ are determined, one knows everything about the MFAEADs. Other experiments, dealing with relatively slow photoelectrons instead of energetic Auger electrons have used a limited partial wave expansion of the outgoing electron wave to simplify the problem. The determination of the limited number of complex amplitudes is usually called the quantum mechanically complete experiment (Motoki *et al* 2002a, 2002b, Geßner *et al* 2002, Lebech *et al* 2003, Teramoto *et al* 2007). In case of the more structured MFAEADs the number of necessary partial waves would be unreasonably large. The elegance of using $F^{(m)}$ functions is the absence of additional assumptions and the straightforward unique determination of $F^{(m)}$ from the measurements, without the need for multi-parameter fitting procedures.

With our experimental apparatus we recorded data to determine the ADs of ions detected in coincidence with Auger electrons emitted in fixed directions. The advantage of using electron spectrometers with a very limited acceptance angle at fixed positions compared to methods using 4π sr collection efficiency is the higher energy resolution obtainable at high kinetic energies. Here this aspect is crucial because we will discuss the differences in the ADs of the electrons in the close-lying h- and the i-band.

Equation (5) is very convenient for a theoretical descriptions of the process, however in the experiment, the roles of the fragment ion and electron are exchanged. We

do not record angular distributions of electrons for a fixed molecular axis, but angular distributions of molecular axes for fixed electron emission directions. In other words, we consider ion intensities in the electron frame (Liu *et al* 2007). In the electron frame, the emission direction of the electron plays the same role as the molecular axis for the molecular frame. Of course the angle θ between the molecular axis and the electron emission direction does not change, but in order to fully describe the direction of the molecular axis in the electron frame, one more angle ϕ_e (instead of ϕ_n) is needed. Again, we use the polarization vector $\vec{E}$ as a reference and define the electron coordinate frame in a way that the electron is emitted along the z-axis. The x, y-axes are defined indirectly by the condition that $\vec{E}$ is in the x, z-plane and has a positive x component. In the degenerate case, where the electron detection direction is along the polarization of the light (here horizontal polarization and electron detector 1) the C^+ intensity distribution can be expressed as a function of θ only $I^e(\theta)$.

We will call the angle between $\vec{e}$ and $\vec{E}\,\theta_e^E$. The intensity distribution of ions in the electron frame is a function of three angles $I^e\left(\theta_e^E, \theta, \phi^e\right)$. Again as a consequence of the dipole approximation this three-dimensional function can be written in terms of four one-dimensional functions: $F_{00}^{(e)}(\theta)$, $F_{20}^{(e)}(\theta)$, $F_{21}^{(e)}(\theta)$ and $F_{22}^{(e)}(\theta)$

$$\begin{aligned} I^e\left(\theta_e^E, \theta, \phi_e\right) &= F_{00}^{(e)}(\theta) + \tfrac{1}{2}\left(3\cos^2\left(\theta_e^E\right) - 1\right) \cdot F_{20}^{(e)}(\theta) \\ &\quad + 3\sin\left(\theta_e^E\right)\cos\left(\theta_e^E\right) \cdot F_{21}^{(e)}(\theta) \cdot \cos(\phi_e) \\ &\quad + 3\sin^2\left(\theta_e^E\right) \cdot F_{22}^{(e)}(\theta) \cdot \cos(2\phi_e). \end{aligned} \tag{6}$$

The mutual angle θ between the electron emission direction and the molecular axis appears in both equations (5) and (6). Moreover the functions $F_{00}^{(m)}(\theta)$ and $F_{00}^{(e)}(\theta)$ have a simple interpretation. $\int_{\theta 1}^{\theta 2} F_{00}^{(m)}(\theta)\sin(\theta)\,\mathrm{d}\theta$ and $\int_{\theta 1}^{\theta 2} F_{00}^{(e)}(\theta)\sin(\theta)\,\mathrm{d}\theta$ describe the probability that electrons are emitted within the angle interval $\theta 1 \leqslant \theta \leqslant \theta 2$ with respect to the molecular axis for a randomly oriented sample of molecules. This can be seen by performing the integrations $\int_0^\pi \sin\left(\theta_n^E\right)\mathrm{d}\theta_n^E \int_0^{2\pi} \mathrm{d}\phi_n$ over equation (5) and performing the integrations $\int_0^\pi \sin\left(\theta_e^E\right)\mathrm{d}\theta_e^E \int_0^{2\pi} \mathrm{d}\phi_e$ over equation (6). In both cases only the terms with F_{00} remain. So it is no big surprise that $F_{00}^{(m)}$ and $F_{00}^{(e)}$ are just two different names for the same function.

As proven in the appendix, there is a relatively simple transformation from the electron frame to the molecular frame. Using equation (7) $F_{00}^{(m)}$, $F_{20}^{(m)}$, $F_{21}^{(m)}$, $F_{22}^{(m)}$ can be calculated directly from $F_{00}^{(e)}$, $F_{20}^{(e)}$, $F_{21}^{(e)}$, $F_{22}^{(e)}$. Thus $F_{00}^{(e)}$, $F_{20}^{(e)}$, $F_{21}^{(e)}$, $F_{22}^{(e)}$ determine the MFAEADs:

$$\begin{aligned} F_{00}^{(m)}(\theta) &= F_{00}^{(e)}(\theta) \\ F_{20}^{(m)}(\theta) &= \frac{3\cos(2\theta)+1}{4} \cdot F_{20}^{(e)}(\theta) + \frac{3}{2} \cdot \sin(2\theta) \cdot F_{21}^{(e)}(\theta) \\ &\quad + 3 \cdot \sin^2(\theta) \cdot F_{22}^{(e)}(\theta) \\ F_{21}^{(m)}(\theta) &= \frac{1}{2} \cdot \sin(2\theta) \cdot F_{20}^{(e)}(\theta) - \cos(2\theta) \cdot F_{21}^{(e)}(\theta) \\ &\quad - \sin(2\theta) \cdot F_{22}^{(e)}(\theta) \\ F_{22}^{(m)}(\theta) &= \frac{1}{4} \cdot \sin^2(\theta) \cdot F_{20}^{(e)}(\theta) - \frac{1}{4} \cdot \sin(2\theta) \cdot F_{21}^{(e)}(\theta) \\ &\quad + \frac{\cos(2\theta)+3}{4} \cdot F_{22}^{(e)}(\theta). \end{aligned} \tag{7}$$

3.4. Experimental determination of the MFAEADs

Some key results of this work are presented as MFAEADs by Rolles *et al* (2008). As we would like to encourage other experimental groups to employ our new method for the determination of resonant Auger electron ADs, we give a rather detailed description of the data evaluation method in the present paper.

For a given light polarization direction (horizontal or vertical), and the electron detection direction (electron spectrometer 1 or 2) and energy interval of the electrons (band i or band h) one can determine the intensity distributions of coincident C^+ ions as a function of two angles: $I^e(\theta, \phi_e)$.

For any fixed value of θ_e^E, equation (6) can be summarized to three one-dimensional functions $H_0(\theta)$, $H_1(\theta)$, $H_2(\theta)$:

$$I^e(\theta, \phi_e) = H_0(\theta) + H_1(\theta) \cdot \cos(\phi_e) + H_2(\theta) \cdot \cos(2\phi_e). \tag{8}$$

The determination of H_0, H_1, H_2 from the measured distributions is sometimes called the 'projection method'. H_0, H_1, H_2 are smooth functions that obey the boundary conditions:

$$H_1(\theta = 0) = H_1(\theta = \pi) = H_2(\theta = 0) = H_2(\theta = \pi) = 0. \tag{9}$$

Furthermore, for any value of θ and ϕ_e, the intensity $I^e(\theta, \phi_e)$ must not be negative. This implies, for example, $H_0(\theta) \geqslant 0$.

For a measured intensity distribution, $I^e(\theta, \phi_e)$, the functions H_0, H_1, H_2 can be directly calculated:

$$\begin{aligned} H_0(\theta) &= \frac{1}{2\pi}\int_0^{2\pi} I^e(\theta, \phi_e)\,\mathrm{d}\phi_e \\ H_1(\theta) &= \frac{1}{\pi}\int_0^{2\pi} I^e(\theta, \phi_e) \cdot \cos(\phi_e)\,\mathrm{d}\phi_e \\ H_2(\theta) &= \frac{1}{\pi}\int_0^{2\pi} I^e(\theta, \phi_e) \cdot \cos(2\phi_e)\,\mathrm{d}\phi_e. \end{aligned} \tag{10}$$

Here the experimental data is essentially a list of M ions. So it is convenient to replace the integration over intensity by the corresponding summation over events. We calculate, for each detected C^+ ion, the values of the momentum coordinates px_i, py_i, pz_i, $(i = 1, \ldots, M)$ and the corresponding angles in the electron frame θ^i and ϕ_e^i. The interval 0 to π of possible values for θ is divided into N intervals $I[j]$ $j = 1, \ldots, N$. In analogy to equations (10) for each index j, we determine those ions with θ^i in the interval $I[j]$ and calculate the sums:

$$\begin{aligned} N_0[j] &= \sum_{i \text{ with } \theta^i \text{ in } I[j]} 1 \\ N_1[j] &= 2 \sum_{i \text{ with } \theta^i \text{ in } I[j]} \cos\left(\phi_e^i\right) \\ N_2[j] &= 2 \sum_{i \text{ with } \theta^i \text{ in } I[j]} \cos\left(2\phi_e^i\right). \end{aligned} \tag{11}$$

Table 2. H-functions determined from the experiment.

Light polarization	Electron detector	H-functions
Horizontal	1	$^{\text{hori}}_{\text{det1}}H_0(\theta)$
Horizontal	2	$^{\text{hori}}_{\text{det2}}H_0(\theta)$, $^{\text{hori}}_{\text{det2}}H_1(\theta)$, $^{\text{hori}}_{\text{det2}}H_2(\theta)$
Vertical	1	$^{\text{vert}}_{\text{det1}}H_0(\theta)$, $^{\text{vert}}_{\text{det1}}H_2(\theta)$
Vertical	2	$^{\text{vert}}_{\text{det2}}H_0(\theta)$, $^{\text{vert}}_{\text{det2}}H_1(\theta)$, $^{\text{vert}}_{\text{det2}}H_2(\theta)$

The condition 'θ^i in $I[j]$' introduces a selection of the ion emission direction. Here we have to consider the size of this selected area on the unit sphere as the intervals near the equator ($\theta = 90°$) contain more intensity than those near the poles ($\theta = 0°$) and ($\theta = 180°$).

The area of the surface of a unit sphere that corresponds to the interval $[Ij]$ is proportional to

$$A[j] = \frac{1}{2}\int_{I[j]} \sin(\theta)\,\mathrm{d}\theta. \tag{12}$$

These areas are normalized such that

$$\sum_j A[j] = 1. \tag{13}$$

The average values of $H_0(\theta)$, $H_1(\theta)$, $H_2(\theta)$ in the interval $I[j\ ]$ are given by the corresponding values of h_0, h_1, h_2:

$$h_0[j] = N_0[j]/A[j], \qquad h_1[j] = N_1[j]/A[j],$$
$$h_2[j] = N_2[j]/A[j]. \tag{14}$$

The h_0, h_1, h_2 are normalized, so that

$$\sum_j h_0\,[j]\cdot A[j] = \text{number of ions}. \tag{15}$$

The values of $H_0(\theta)$, $H_1(\theta)$, $H_2(\theta)$ for any value of θ can be derived from interpolating the values of h_0, h_1, h_2. Only close to $\theta = 0$ and $\theta = \pi$ additional points should be used to enforce the boundary conditions (9).

In this way the information from the experiment can be summarized in the functions H_0, H_1, H_2 for each combination of the light polarization and electron detector. The third column of table 2 shows a list of these functions. The 'missing' functions $^{\text{hori}}_{\text{det1}}H_1[\theta]$, $^{\text{hori}}_{\text{det1}}H_2[\theta]$, $^{\text{vert}}_{\text{det1}}H_1[\theta]$ are zero for symmetry reasons. The nine non-zero functions are not completely independent but should be interrelated by equation (6). As they come from different measurements with different acquisition times, gas destiny etc. their total intensities are not yet consistent. In order to remove these inconsistencies we first normalize them, i.e. we multiply all functions in one line of table 2 by a common factor. This factor is given by

$$\left(1 + \beta\cdot\frac{3\cdot\cos^2\left(\theta_e^E\right) - 1}{2}\right) / (2\pi\int_0^\pi H_0(\theta)\sin(\theta)\,\mathrm{d}\theta), \tag{16}$$

where θ_e^E is the angle between the light polarization and the electron detector of the corresponding measurement, β is the electron anisotropy parameter, $\left(1 + \beta\cdot\frac{3\cdot\cos^2(\theta_e^E)-1}{2}\right)$ is proportional to the electron count rate expected from the electron angular distribution and $\left(2\pi\int_0^\pi H_0(\theta)\sin(\theta)\,\mathrm{d}\theta\right)$ is the angle integrated measured intensity of the corresponding electron–ion coincidences. This normalization ensures that the total intensity of coincident ions follows the angular distribution of Auger electrons. We estimated the experimental values of β from figure 4 of (Kukk *et al* 1999): i-band: $\beta = 0.02 \pm 0.05$. h-band: $\beta = -0.33 \pm 0.05$. To distinguish the normalized H-functions from the others we call them $^{\text{hori}}_{\text{det1}}\widetilde{H}_0(\theta)$ instead of $^{\text{hori}}_{\text{det1}}H_0(\theta)$ etc.

After normalization, all the functions listed in table 2 should be related to four functions $F_{00}^{(e)}(\theta)$, $F_{20}^{(e)}(\theta)$, $F_{21}^{(e)}(\theta)$, $F_{22}^{(e)}(\theta)$ according to equation (6). For a set of measurements including different detectors and light polarization directions the definition of θ_e^E needs some care. The choice of the sign of the direction vector $\vec{E}$ of the linear polarization of light is, of course, arbitrary but must be consistent for all measurements, while the choice of the direction vector $\vec{e}$ of the electron detector position is unique. Here we chose $\vec{E}$ towards the first electron spectrometer for the horizontal polarization and upwards for the vertical polarization. θ_e^E is given by

$$\theta_e^E = \arccos(\vec{E}\,,\,\vec{e}\,). \tag{17}$$

So the four different angles for the four rows of table 2 are 0°, 125.3°, 90° and 144.7° respectively and not 0°, 54, 7°, 90° and 35.3°. By comparing equation (6) with equation (8) we can derive two redundant equations for the determination of $F_{00}^{(e)}(\theta)$: two for $F_{20}^{(e)}(\theta)$, two for $F_{21}^{(e)}(\theta)$ and three for $F_{22}^{(e)}(\theta)$:

$$F_{00}^{(e)}(\theta) = lk1(\theta) = lk2(\theta)$$
$$F_{20}^{(e)}(\theta) = lk3(\theta) = lk4(\theta)$$
$$F_{21}^{(e)}(\theta) = lk5(\theta) = lk6(\theta)$$
$$F_{22}^{(e)}(\theta) = lk7(\theta) = lk8(\theta) = lk9(\theta)$$
$$lk1(\theta) \equiv {}^{\text{hori}}_{\text{det2}}\widetilde{H}_0(\theta),$$
$$lk2(\theta) \equiv \tfrac{1}{2}\cdot{}^{\text{vert}}_{\text{det1}}\widetilde{H}_0(\theta) + \tfrac{1}{2}\cdot{}^{\text{vert}}_{\text{det2}}\widetilde{H}_0(\theta)$$
$$lk3(\theta) \equiv {}^{\text{vert}}_{\text{det2}}\widetilde{H}_0(\theta) - {}^{\text{vert}}_{\text{det1}}\widetilde{H}_0(\theta),$$
$$lk4(\theta) \equiv {}^{\text{hori}}_{\text{det1}}\widetilde{H}_0(\theta) - {}^{\text{hori}}_{\text{det2}}\widetilde{H}_0(\theta)$$
$$lk5(\theta) \equiv -\tfrac{1}{\sqrt{2}}\cdot{}^{\text{hori}}_{\text{det2}}\widetilde{H}_1(\theta), \qquad lk6(\theta) \equiv -\tfrac{1}{\sqrt{2}}\cdot{}^{\text{vert}}_{\text{det2}}\widetilde{H}_1(\theta)$$
$$lk7(\theta) \equiv {}^{\text{vert}}_{\text{det2}}\widetilde{H}_2(\theta), \qquad lk8(\theta) \equiv \tfrac{1}{2}\cdot{}^{\text{hori}}_{\text{det2}}\widetilde{H}_2(\theta),$$
$$lk9(\theta) \equiv \tfrac{1}{3}\cdot{}^{\text{vert}}_{\text{det1}}\widetilde{H}_2(\theta). \tag{18}$$

In general there is only one choice for the value of β used for the normalization factor in equation (16) to fulfil the first four equations in (18). Strictly speaking, β can be determined as a byproduct from our measurement. However the values given by Kukk *et al* (1999) are certainly more precise, therefore we use these values.

Looking at equations (18) using only the data obtained with horizontally polarized radiation one can still calculate all $F^{(e)}$ functions. The measurements using vertical polarization provide a valuable consistency check of the experimental data and the formulae used.

After checking the consistency of $lk1(\theta)$ to $lk9(\theta)$, we determine $F_{00}^{(e)}(\theta)$, $F_{20}^{(e)}(\theta)$, $F_{21}^{(e)}(\theta)$, $F_{22}^{(e)}(\theta)$ by weighted averaging over the corresponding lk-values. Figure 4 shows the results for the h-band. These four functions summarize the full information obtained in the experiment. Figure 5 shows the corresponding results for the i-band.

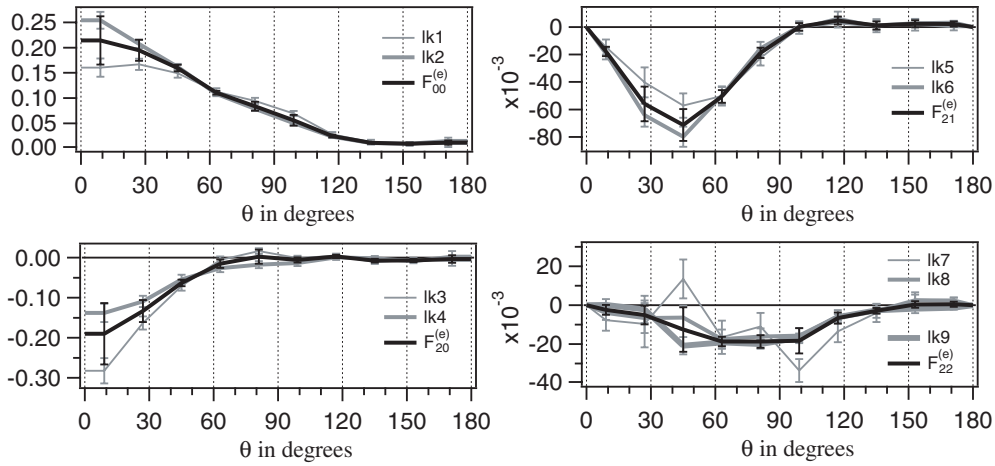

Figure 4. $F^{(e)}(\theta)$ functions derived from the measured H functions for the h-band.

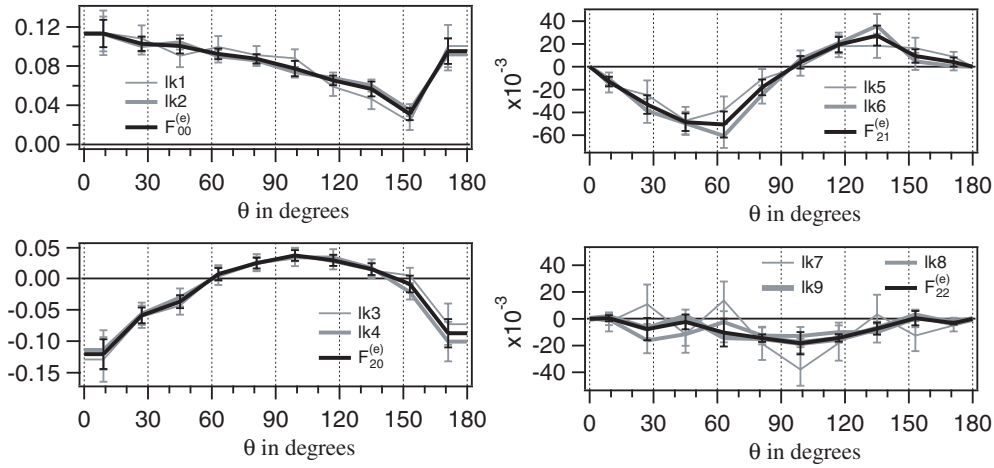

Figure 5. $F^{(e)}(\theta)$ functions derived from the measured H functions for the i-band.

Using equation (7) the electron-frame F-functions can be transformed into four functions $F_{00}^{(m)}(\theta)$, $F_{20}^{(m)}(\theta)$, $F_{21}^{(m)}(\theta)$, $F_{22}^{(m)}(\theta)$. The result of this transformation is shown in figure 6 together with the corresponding theoretical $F^{(m)}$ functions derived from the theoretical predictions based on table 1 and equations (2), (3), (4) and (5).

As the F-functions summarize the complete information on the process, they are also a convenient way to compare experiment and theory. One of the approximations used by theory is to neglect the non-resonant part of the cross section. Considering the strength of the resonance visible in total electron yield measurements in figure 2 of Piancastelli *et al* (1997) this is certainly a good approximation. The selection rules for the excitation lead to two predictions: $F_{20}^{(m)} = -F_{00}^{(m)}$, meaning that molecules with their axes parallel to the electric vector cannot be excited at all and $F_{21}^{(m)} = 0$ which has no such simple geometrical interpretation. Looking at the datapoints in figure 6 one can see that the first prediction is fulfilled within the experimental error bars for both bands. We observe a small but negative $F_{21}^{(m)}$ function in the experiment for both bands but we cannot exclude systematic experimental errors as the source for such small deviations from zero. The overall agreement of theory and experiment is excellent for the h-band. For the i-band theory and experiment show deviations, however the main features are predicted correctly. One very interesting prediction of theory is that the ADs of the h-bands and i-bands differ very much. In particular the electrons from the h-band are expected to fly preferentially in the same direction like the C^+ ion (high intensity for $\theta = 0^\circ$ and very low intensity for $\theta = 180^\circ$). For the i-band this C–O asymmetry is smaller. In the theoretical prediction, the $F_{21}^{(m)}$ function is zero and the $F_{22}^{(m)}$ function is very small, so in theory the MFAEADs are almost cylinder symmetric around the molecular axis, while the experimental result indicates a slight dependence on the electric vector as $F_{22}^{(m)}$ is not exactly zero.

In order to give a more direct illustration of the comparison of experiment and theory, we show images of the 3D MFAEADs in figure 7 for the case where the molecular axis is perpendicular to the electric vector $\left(\theta_n^E = 90^\circ\right)$. In that case

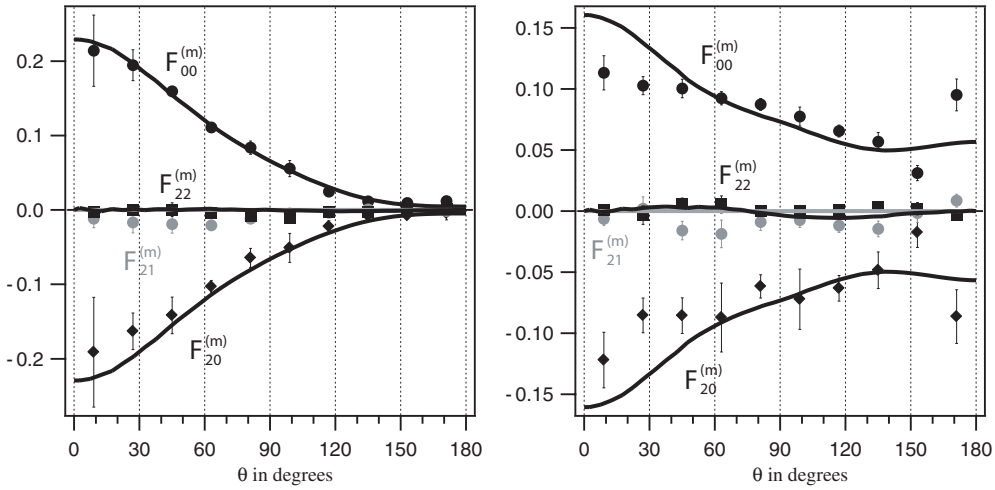

Figure 6. Comparison of experimental F-functions (data points) and theoretical predictions (solid curves). The left panel shows the results for the h-band. The right panel for the i-band. The upper curves are $F_{00}^{(m)}$, the lower curves are $F_{20}^{(m)}$. The curves near the zero line are $F_{21}^{(m)} = 0$ (grey) and $F_{22}^{(m)}$ (black).

equation (5) simplifies to

$$I^m\left(\theta_n^E = 90^0, \theta, \phi_n\right) = F_{00}^{(m)}(\theta) - \tfrac{1}{2} \cdot F_{20}^{(m)}(\theta) + 3 \cdot F_{22}^{(m)}(\theta) \cdot \cos(2\phi_n). \quad (19)$$

As no error bars are shown in this plot, one tends to overestimate the differences of theory and experiment. In particular the deviations from the cylindrical shape of the experimental distributions perpendicular to the molecular axis is not beyond the error bars of the corresponding data points of the F-functions. In the experimental data for the i-band one can see a peaked intensity in the direction opposite to the C-atom. This is probably a lens effect of the molecular potential. It corresponds to large values of $F_{00}^{(m)}$ and $F_{20}^{(m)}$ near $\theta = 180^\circ$. The biggest difference of experiment and theory occurs for the i-band. This may be due to an overestimation of the contribution of the $4^2\Pi$ state. However, all features predicted by theory were confirmed experimentally. The overall agreement is surprisingly good.

In order to answer the second question, if the MFAEADs depend on the vibrational level of the excited state, we measured the distributions of the molecules for the first variationally excited state using horizontal polarization with similar statistics as for the vibrational ground state. As mentioned above, even without the measurement using vertical polarization it is still possible to deduce the F-functions from the measured H-functions and to determine the MFAEADs. When changing the photon energy, we observe a slight change in the position of the width of the h-band. This effect is theoretically understood and in good agreement with the high-resolution data of Piancastelli and coworkers (Piancastelli *et al* 1997). The corresponding data are shown in figure 8(a).

For the ions the most pronounced difference between $v = 0$ and $v = 1$ is the kinetic energy of the C^+ detected in coincidence with electrons in the h-band shown in figure 8. The second peak at about 3 eV kinetic energy visible for the vibrational ground state disappears for the resonant excitation to $v = 1$ indicating that the dissociation depends critically

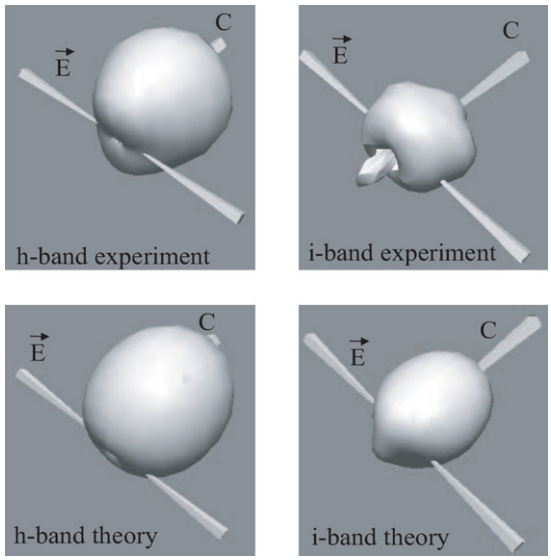

Figure 7. Electron intensity in the molecular frame. Comparison of experiment and theory.

on the nuclear coordinates. Nevertheless, the ADs of the C^+ ions with kinetic energies between 1.0 and 6 eV were found to be identical to those of the vibrational ground state. Thus the MFAEADs must also be identical. Apparently the difference in the initial nuclear coordinates does not translate into a difference of the MFAEADs, it only affects the branching ratios into the Auger final states and the dissociation pathways.

A similar result was found for the dependence on the KER of the C^+ ions. We divided the data set for the h-band for the vibrational ground state into two parts according to the two peaks at 1.5 and 3 eV in the KER spectrum of C^+ ions and analysed them separately. Again the ADs for the two cases did not show any significant differences.

The vibrational excitation has a strong influence on both the electron spectrum and the kinetic energy release. Therefore

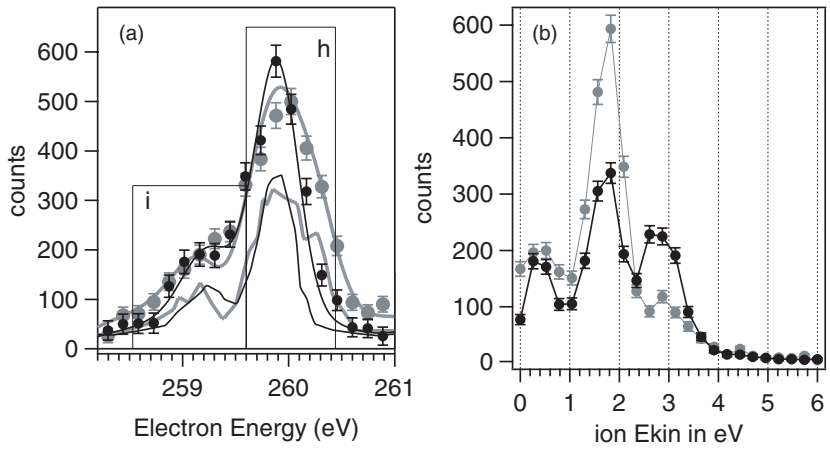

Figure 8. (a) Comparison of the spectra of electrons detected by electron detector 2 at different photon energies for horizontal light polarization. The black data points are from our coincidence measurement at h$\nu = 287.40$ eV, i.e. for the excitation to the vibrational ground state $\nu = 0$. The grey data points show our results at h$\nu = 287.66$ eV, i.e. for the excitation to $\nu = 1$. The lower black line shows the high-resolution data of Piancastelli and coworkers (Piancastelli *et al* 1997), scaled arbitrarily. To mimic the effect of our lower instrumental resolution we convoluted the data with a 300 meV FWHM Gaussian profile (upper black line). This value gives the best overall agreement with our measured electron spectrum. (b) Comparison of the corresponding kinetic energy distributions of C^+ ions detected in coincidence with electrons in the h-interval.

it is surprising that the ADs of the Auger electrons stay the same. As we clearly see the effects on the electron spectrum and the kinetic energy release, we can rule out experimental mistakes. We only give a tentative qualitative interpretation for the stability of the MFAEADs here. The MFAEADs are determined by the shape of the orbitals involved and the scattering of Auger electrons in the molecular potential. It is possible that both factors do not depend as critically on the internuclear distance as the Auger transition matrix elements and the dissociation dynamics do.

4. Conclusion

In this work we demonstrated that the ADs of the Auger electrons belonging to the h-band show a very pronounced asymmetry with respect to the molecular axis of CO, while the Auger electrons belonging to the i-band have a more symmetric AD. This observation is a confirmation of theoretical predictions based on the two-step model and the relatively simple one-centre approach including phase shifts due to the molecular potential. The overall agreement with the theoretical predictions is surprisingly good. We did not observe any influence of the nuclear motion on the MFAEADs, neither via the kinetic energy release nor via the vibrationally excited state. In this showcase example, we demonstrated the power of the new experimental method in which ADs of ions are transformed into MFAEADs. These ions are detected in coincidence with electrons that are energy analysed using two high-resolution electron spectrometers mounted in fixed directions.

Acknowledgments

The authors are grateful to the staff of the ALS for their help in conducting this experiment, in particular to T Young, E Ahrenholz, A Aguilar, R Bilodeau and D Kilcoyne. This work was supported by the Office of Basic Energy Sciences, US Department of Energy, Chemical Sciences, Geosciences and Biosciences Division, Grants-in-Aid for Scientific Research from the Japanese Society for the Promotion of Science (JSPS), and the Japanese Ministry of Education, Culture, Sports, Science and Technology. D R acknowledges support from the Alexander von Humboldt foundation through the Feodor Lynen program, X J L acknowledges support from JSPS and A N G acknowledges JSPS and Tohoku University for support and Tohoku University for hospitality during his stays.

Appendix

Proof of equation (7): in the notation we used in Liu *et al* (2007), the transformation from electron frame to molecular frame can be explicitly written for the expansion coefficients for the spherical harmonics expansion as

$$H^{(\mathrm{m})}_{J''JN'} = \sum_{\substack{0\leqslant J' \\ -\min(J,J')\leqslant N\leqslant\min(J,J')}} (-1)^N \sqrt{\frac{2J'+1}{2J''+1}} \langle J, J', -N', 0 \mid J'', -N' \rangle \times \langle J, J', -N, N \mid J', 0 \rangle H^{(\mathrm{e})}_{J'JN}$$

and for the expansion coefficients for the Legendre polynomial expansion as

$$C^{(\mathrm{m})}_{J''JN'} = \sum_{\substack{0\leqslant J' \\ 0\leqslant N\leqslant\min(J,J')}} (-1)^N \frac{1+(-1)^{J+J'+J''}}{1+\delta_{N',0}} \times \left[\frac{(J'+N)!(J+N)!(J''-N')!(J-N')!}{(J'-N)!(J-N)!(J''+N')!(J+N')!}\right]^{1/2} \times \left\langle J, J', -N', 0 \;\middle|\; J'', -N' \right\rangle \left\langle J, J', -N, N \;\middle|\; J'', 0 \right\rangle C^{(\mathrm{e})}_{J'JN}.$$

Then the corresponding transformation for the F_{JN} functions becomes

$$F^{(m)}_{JN'}(\theta) = \sum_N T^J_{N'N}(\theta)\, F^{(e)}_{JN}(\theta)$$

$$T^J_{N'N}(\theta) = \left[\frac{(J-N')!(J+N)!}{(J+N')!\,(J-N)!}\right]^{1/2} \frac{(-1)^N}{1+\delta_{N',0}}$$

$$\times\left[d^J_{-N',-N}(\theta) + (-1)^{N'} d^J_{N',-N}(\theta)\right]$$

where the rotation functions $d^J_{N',N}(\theta)$ are as defined on page 85 of (Zare 1988).

References

Berrah N, Langer B, Wills A A, Kukk E, Bozek J D, Farhat A and Gorczyca T W 1999 *J. Elect. Spec. Rel. Phen.* **101–103** 1–11

Bonhoff S, Bonhoff K and Blum K 1999 *J. Phys. B: At. Mol. Opt. Phys.* **32** 1139–49

Bonhoff S, Bonhoff K, Schimmelpfennig B and Nestmann B 1997 *J. Phys. B: At. Mol. Opt. Phys.* **30** 2821–34

Botting S K and Lucchese R R 1997 *Phys. Rev.* A **56** 3666–74

Dörner R *et al* 1998 *Phys. Rev. Lett.* **81** 5776–9

Downie P and Powis I 1999 *Phys. Rev. Lett.* **82** 2864–7

Edwards A K, Zheng Q, Wood R M and Mangan M A 1997 *Phys. Rev.* A **55** 4269–72

Feifel R *et al* 2002 *Phys. Rev.* A **65** 052701

Feyer V, Bolognesi P, Coreno M, Prince K C, Avaldi L, Jansik B and Carravetta V 2007 *J. Phys. B: At. Mol. Opt. Phys.* **40** F35–42

Fink R F, Piancastelli M N, Grum-Grzhimailo A N and Ueda K 2008 *J. Chem. Phys.* submitted

Geßner O, Hikosaka Y, Zimmermann B, Hempelmann A, Lucchese R R, Eland J H D, Guyon P and Becker U 2002 *Phys. Rev. Lett.* **88** 193002

Golovin A V, Cherepkov N A and Kuznetsov V 1992 *Z. Phys.* D **24** 371–5

Golovin A, Heiser F, Quayle C, Morin P, Simon M, Gessner O, Guyon P and Becker U 1997 *Phys. Rev. Lett.* **79** 4554–7

Guillemin R, Shigemasa E, Le Guen K, Ceolin D, Miron C, Leclercq N, Morin P and Simon M 2001 *Phys. Rev. Lett.* **87** 203001

Heiser F, Geßner O, Viefhaus J, Wieliczek K, Hentges R and Becker U 1997 *Phys. Rev. Lett.* **79** 2435–7

Hemmers O, Heiser F, Eiben J, Wehlitz R and Becker U 1993 *Phys. Rev. Lett.* **71** 987–90

Kukk E, Bozek J, Cheng W, Fink R, Wills A and Berrah N 1999 *J. Chem. Phys.* **111** 9642–50

Kuznetsov V V and Cherepkov N A 1996 *J. Electron. Spectrosc. Relat. Phenom.* **79** 437–40

Lebech M, Houver J and Dowek D 2002 *Rev. Sci. Instrum.* **73** 1865–74

Lebech M, Houver J C, Lafosse A, Dowek D, Alcaraz C, Nahon L and Lucchese R R 2003 *J. Chem. Phys.* **118** 9653

Liu X, Lucchese R R, Grum-Grzhimailo A N, Morishita Y, Saito N, Prümper G and Ueda K 2007 *J. Phys. B: At. Mol. Opt. Phys.* **40** 485–96

Lucchese R R, Lafosse A, Brenot J C, Guyon P M, Houver J C, Lebech M, Raseev G and Dowek D 2002 *Phys. Rev.* A **65** 020702

Motoki S, Adachi J, Ito K, Ishii K, Soejima K, Yagishita A, Semenov S K and Cherepkov N A 2002a *J. Phys. B: At. Mol. Opt. Phys.* **35** 3801–19

Motoki S, Adachi J, Ito K, Ishii K, Soejima K, Yagishita A, Semenov S K and Cherepkov N A 2002b *Phys. Rev. Lett.* **88** 063003

Osborne S J, Sundin S, Ausmees A, Sorensen S L, Kikas A and Svensson S 1998 *J. Electron. Spectrosc. Relat. Phenom.* **95** 25–36

Piancastelli M N, Neeb M, Kivimäki A, Kempgens B, Köppe H M, Maier K and Bradshaw A M 1996 *Phys. Rev. Lett.* **77** 4302–5

Piancastelli M N, Neeb M, Kivimäki A, Kempgens B, Köppe H M, Maier K, Bradshaw A M and Fink R F 1997 *J. Phys. B: At. Mol. Opt. Phys.* **30** 5677–92

Prümper G, Lischke T, Fukuzawa H and Ueda K 2007 *Rev. Sci. Instrum.* **78** 083104–1

Prümper G and Ueda K 2007 *Nucl. Instrum. Methods Phys. Res.* A **574** 350–62

Rolles D, Pesic Z, Perri M, Bilodeau R, Ackerman G, Rude B, Kilcoyne A, Bozek J and Berrah N 2007 *Nucl. Instrum. Methods Phys. Res.* B **261** 170–4

Rolles D, Prümper G, Fukuzawa H, Liu X-J, Fink R, Grum-Grzhimailo A N, Pešić Z D, Dumitriu I, Berrah N and Ueda K 2008 *Phys. Rev. Lett.* submitted

Rolles D *et al* 2005 *Nature* **437** 711–5

Semenov S K, Kuznetsov V V, Cherepkov N A, Bolognesi P, Feyer V, Lahmam-Bennani A, Casagrande M E S and Avaldi L 2007 *Phys. Rev.* A **75** 032707

Shigemasa E, Adachi J, Oura M and Yagishita A 1995 *Phys. Rev. Lett.* **74** 359–62

Svensson S, Carlsson-Göthe M, Karlsson L, Nilsson A, Mårtensson N and Gelius U 1991 *Phys. Scr.* **44** 184–90

Teramoto T, Adachi J, Hosaka K, Yamazaki M, Yamanouchi K, Cherepkov N A, Stener M, Decleva P and Yagishita A 2007 *J. Phys. B: At. Mol. Opt. Phys.* **40** F241–50

Weber T *et al* 2003 *Phys. Rev. Lett.* **90** 153003

Weber T *et al* 2004 *Nature* **431** 437–40

Westerveld W B, van der Weg J, van Eck J, Heideman H G M and West J B 1996 *Chem. Phys. Lett.* **252** 107–11

Zähringer K, Meyer H and Cederbaum L S 1992a *Phys. Rev.* A **46** 5643–52

Zähringer K, Meyer H and Cederbaum L S 1992b *Phys. Rev.* A **45** 318–28

Zare R 1988 *Angular Momentum* (New York: Wiley) p 85